

RESEARCH ARTICLE

Open Access



# Designing 3D-printed concrete structures with scaled fabrication models

Yefan Zhi<sup>1</sup>, Teng Teng<sup>1</sup> and Masoud Akbarzadeh<sup>1,2\*</sup>

## Abstract

This article proposes using scaled fabrication models to assist the design research of 3D-printed discrete concrete structures where full-scale fabrication tests are costly and time-consuming. A scaled fabrication model (SFM) is a scaled model 3D-printed the same way as in actual construction to reflect its fabrication details and acquire alike layer line textures. The components of a 1:10 SFM can be easily produced by consumer-level desktop 3D printers with minimal modification. SFMs assist the design communication and make possible quick tests of distinct fabrication designs that are hard to assess in digital modeling during the conceptual design phase. A case study of a discrete compression-dominant funicular floor derived from graphic statics is presented to illustrate the contribution of SFM to the design research of force-informed toolpathing where the printing direction of a component is aligned to the principal stress line. The design iterations encompass a sequence of component, partial, and full model SFM printing tests to explore and optimize the fabrication schemes where parallel, non-parallel, and creased slicing methods to create toolpaths are compared and chosen to adapt different discrete components.

**Keywords** 3D printing, Scaled fabrication model, Graphic statics, Force-informed toolpathing

## 1 Introduction

Architectural additive manufacturing, or 3D printing revolutionizes the way buildings can be designed and constructed. The technology's ability to create freeform, complex geometry gives architects a higher degree of freedom to realize innovative designs that could either enhance the structural performance or produce unique aesthetics (Khoshnevis, 2004; Paolini et al., 2019; van Woensel, van Oirschot, Burgmans, Mohammadi, & Hermans, 2018). To explore its strength in creating large-scale efficient structures (walls, beams, bridges, etc.), we are looking into discrete systems where each component is printed separately and then assembled (Fig. 1).

While 3D-printed discrete systems provide compelling construction solutions in the cases of Fig. 1, they also bring challenges to aspects such as discretization design, toolpath rationalization, joint design, and material deposition control which require careful investigations from the designers. Digital visualization and simulation of 3D printed systems have been a primitive tool for them to rationalize the fabrication design. Still it provides limited information on the fabrication challenges and can not predict possible production defects at early stages. On the other hand, a complete full-scale construction test involves the preparation and transportation of concrete, the printing of the components in factories or labs, component transportation, and in-situ assembly (Xiao, Ji, et al., 2021). The significant time, material, energy, and labor costs restrict architects and engineers from efficiently conducting tests essential to design development and rationalization.

\*Correspondence:

Masoud Akbarzadeh  
masouda@design.upenn.edu

<sup>1</sup> Polyhedral Structures Laboratory, School of Design, University of Pennsylvania, Philadelphia, PA 19104, USA

<sup>2</sup> Automation, Sensing and Perception (GRASP) Lab, School of Engineering and Applied Science, General Robotic, University of Pennsylvania, Philadelphia, PA 19104, USA





**Fig. 1** Discrete 3D printed architectural systems: (a) Post-tensioned concrete beam (Vantighem et al., 2020); (b) Multi-span post-tensioned concrete bridge (Ahmed, Wolfs, Bos, & Salet, 2022); (c) Post-tensioned concrete bridge (Ooms et al., 2022); (d) Unreinforced concrete masonry footbridge (Bhooshan, 2022); (e) Post-tensioned concrete bridge (Li et al., 2024); and (f) Post-tensioned concrete pavilion (Wu et al., 2022)

### 1.1 3D-printed smooth models

While current commercial/consumer-level desktop 3D printing is extensively exploited as a way to produce physical models for design research and presentation purposes (Jain & Kuthe, 2013), there is a mismatch between that and the construction-scale concrete 3D printing paradigm for producing architectural structures (Bos et al., 2016; Gosselin et al., 2016).

Desktop 3D printers typically use thermoplastic filaments such as PLA, PET-G, and ABS and extrude at a fine resolution of around 0.2 mm layer thickness to produce models with smooth surfaces. They recreate the desired shapes but do not demonstrate the fabrication details and layer line textures inherent to actual construction scale printing.

The toolpaths generated by commercial slicing software (e.g. Cura, Slic3r) for these desktop thermoplastic printers are often far different from those of the structural components printed in industrial gantry or robotic

setups. They make frequent start-and-stops in extrusion and print with high overhang angles incompatible with concrete printing. Thus the successful production of smooth models does not support the viability of the actual fabrication proposal. Furthermore, one component can be converted into different toolpaths under different printing schemes (orientation, slicing method, sectional dimensions, etc.) in construction and results in different forms. Such variations cannot be reflected by desktop models as tuning their printing parameters only results in minimal differences. Thus slicing and printing with current desktop 3D printers can contribute little to design iterations related to the actual fabrication.

### 1.2 Design with scaled fabrication models

To facilitate and accelerate the design iterations in 3D-printed discrete system construction, this study proposes a design-to-fabrication research paradigm that

utilizes 3D-printed scaled fabrication models instead of the smooth models mentioned above. A scaled fabrication model (SFM) is a scaled model that is fabricated the same way as in real construction. In our case, it is a model 3D printed using the toolpath that would also apply to the actual production, and its sectional dimensions (width and height) are also decided by scaling the actual production. SFMs effectively contribute to design decisions for the following reasons:

1. SFMs are easy to produce. As will be shown in Sect. 2, the setup is easily established by modifying a commercially available desktop printer. Toolpaths for construction-scale gantry 3D printers can be easily scaled down to adapt to desktop material extrusion printers by the scale of 1:10 and vice versa, requiring little additional effort in preparing the machine codes for printing. Printing in the desktop scale uses only one person and significantly saves time, material, energy, and labor compared to the construction scale.
2. Unlike computer simulations, physical mockups can provide tactile feedback and reveal subtleties related to spatial relations, aesthetics, and material behaviors that may not be fully captured digitally (Viswanathan & Linsey, 2011). Compared with smooth models, SFMs also carry the same texture as actual construction-scale prints since the geometric parameters are scaled down from the construction scheme. It enables fast realizations of design prototypes at a low cost. Architects, engineers, and researchers can fabricate and test numerous designs and share them with clients in a matter of days if needed (Sharif & Gentry, 2015).
3. Mocking up architectural structures on a smaller scale using desktop 3D printers could also provide a tangible method of testing and optimizing the construction process before actual implementation, complementing computer simulations (De Luca et al., 2006). In preparing SFMs instead of smooth models, designers are asked practical questions such as what is the sectional dimension and how the prints fit with joinery and reinforcements. By exploring different printing schemes of the SFM, one effectively tests that of the actual production in terms of slicing and toolpathing options as well as sectional dimension choices. The concrete mixture consists of coarse aggregates and is hard for small-scale printing. Therefore, SFMs use thermoplastic filaments or clay to replicate the geometrical parameters on the desktop scale. Although the material property is different, SFM can reveal fabrication defects related to the geometric form such as collision, extreme overhang, extreme angles, etc. It is a handy troubleshooting






tool for the fabrication rationalization of the discrete structural components. Furthermore, it also offers an opportunity to test the tectonics of the structural assembly.

The SFM serves as an intermediate tool from geometry-centered design to fabrication-oriented design. It contributes to the conceptual design phase by outlining the limits of 3D-printed concrete structures. Once a design has been validated using the SFM method, it is anticipated that full-scale tests will experience fewer errors. However, we acknowledge that aspects related to the construction such as the lifting of the components and assembly errors might not be fully captured in the SFM stage. Table 1 showcases a series of models produced for the design and fabrication research of a structural component in a parallel study where the proposed method plays a vital role. Between the plain smooth model (Table 1a) and the final production (Table 1e), three different specifications are adopted for scaled model productions. The geometry has been adjusted through the sequential process.

- The 1:10 SFM (Table 1b) uses thermoplastic filaments or clay and is sliced and printed as proposed in Sect. 2. It is a 1:10 scaled model whose sectional dimension ( $3 \times 1$  mm) is determined by that of the original concrete production ( $30 \times 10$  mm) and thus truthfully reflects the final fabrication details and layer line textures.
- The 1:10 material model (Table 1c) utilizing desktop concrete printing is also convenient to produce and helps to understand the printability limits in concrete 3D printing. It is also a strong candidate for strength tests. However, the coarse aggregates in the concrete mixture make it impossible to print with a to-scale section of  $3 \times 1$  mm. It thus does not reflect the final appearance of the print.
- The 1:2 fabrication model (Table 1d) uses the same print section as the full-scale production. The refined results indicate the viability of the final production. The model can be used for strength tests as well as loading tests when assembled. However, it is a practical option only when the design is finalized in all aspects due to the costly printing process and should supersede the design iterations using SFMs.

This article focuses on the method of scaled fabrication model (Table 1b) which is a crucial step in moving from geometrical design to fabrication research. It gathers useful information related to both aesthetics and fabrication and paves way for larger tests suitable for structural performance tests, further underscoring the real-world

**Table 1.** A similar geometry from a parallel study printed in different materials and scales

Print Result	Specifications	Objectives
(a) 	<p><b>1:10 Smooth model</b></p> <ul style="list-style-type: none"> <li>• Material: thermoplastic filaments</li> <li>• Print section: 0.8×0.2 mm</li> <li>• Sliced and printed by commercial software and printer</li> </ul>	<ul style="list-style-type: none"> <li>• Rapid model production without access to our setup</li> </ul>
(b) 	<p><b>1:10 Scaled Fabrication model</b></p> <ul style="list-style-type: none"> <li>• Material: thermoplastic filaments or clay</li> <li>• Print section: 3 × 1 mm</li> <li>• Sliced and printed as proposed in this article</li> </ul>	<ul style="list-style-type: none"> <li>• Rapid model production</li> <li>• Texture examination</li> <li>• Printability test related to geometry</li> </ul>
(c) 	<p><b>1:10 Material model</b></p> <ul style="list-style-type: none"> <li>• Material: concrete</li> <li>• Print section: 5 × 1 mm</li> <li>• Sliced and printed as proposed in this article</li> </ul>	<ul style="list-style-type: none"> <li>• Rapid model production</li> <li>• Printability test related to material property (rheology, curing, etc.)</li> <li>• Strength tests</li> </ul>
(d) 	<p><b>1:2 Fabrication model</b></p> <ul style="list-style-type: none"> <li>• Material: concrete</li> <li>• Print section: 30 × 10 mm</li> <li>• Sliced as proposed in this article, printed by a robotic arm</li> </ul>	<ul style="list-style-type: none"> <li>• Printability test related to material property (rheology, curing, etc.)</li> <li>• Strength tests</li> <li>• Connection and assembly tests</li> <li>• Loading tests</li> </ul>
(e) 	<p><b>1:1 Final production</b></p> <ul style="list-style-type: none"> <li>• Material: concrete</li> <li>• Print section: 30 × 10 mm</li> <li>• Sliced as proposed in this article, printed by a gantry system</li> <li>• Credit: Sika Switzerland</li> </ul>	

applicability of our research. This intermediate process materializes the complex design of architectural components via additive manufacturing, streamlining the design-fabrication procedure.

### 1.3 Scope of the study

This article explores the advantages of designing 3D-printed concrete structures with SFM. Firstly, it will offer an accessible and functional setup for printing SFM on a 1:10 scale. Secondly, it will illustrate the SFM-assisted design strategy using the case study of a compression-dominant discrete funicular floor designed for

concrete 3D printing construction. The case study will involve design iterations that explore the realization of efficient toolpaths based on the form-finding results from graphic statics. Different slicing methods, as the core of fabrication rationalization, will be investigated. Lastly, an operative framework will be summarized.

## 2 Methodology

### 2.1 Desktop-scale printing setup for SFM

Desktop-scale SFM can be handily produced by our accessible, affordable, and versatile setup. Commercial/consumer-level 3D printers usually print at fine

resolutions to create smooth surfaces as they are desired for general purposes. The nozzles used usually have a 0.4 mm diameter with a cross-section of  $0.13 \text{ mm}^2$  and print at the layer height between 0.1 and 0.3 mm. On the other hand, typical concrete 3D printing uses a layer height of 10 mm. We propose that the scale of SFM be 1:10 as smaller than that the layer line textures will be hard to capture and bigger than that it would be hard to print with regular filaments of 1.75 mm diameter. On the 1:10 scale, the  $30 \times 10 \text{ mm}$  concrete section becomes  $3 \times 1 \text{ mm}$  with an area of  $3 \text{ mm}^2$  which is too large for the 0.4 mm nozzle. This issue is solved by simply replacing the default nozzle with a commercially available 1 mm diameter nozzle with a cross-section of  $0.79 \text{ mm}^2$ . Niknafs Kermani, Advani, and Férec (2023)'s simulation suggests that 1 mm layer height complies with 1 mm nozzle diameter.

Our setup is a Creality CR-10 printer with a 1 mm nozzle replacement. CR-10 has a remote extruder fixed on the gantry beam. We replaced it with a direct extruder attached to the hotend which improves material flow control and minimizes issues from retraction in our case of thick layer printing. As the sectional area of the print increases, both the extrusion speed and the nozzle travel speed should slow down to allow successful feeding and deposition of the filament. According to our printing experiments, the print reaches the best extrusion quality when the travel speed of the nozzle is 1.6 mm/sec.

The material of choice for our experiment is polyethylene terephthalate glycol-modified (PET-G) filament. Other thermoplastic filaments also fit our setup. We are also capable of printing clay with the same sectional dimensions using a syringe and auger feeder.

## 2.2 Design with graphic statics

In this research, the advantages of desktop-scale SFM is illustrated in a case study of a funicular floor system, designed utilizing graphic statics. Graphic statics is the study of efficient structural forms utilizing graphical representations (Akbarzadeh, 2016). Polyhedron-based 3D graphic statics, as implemented in this research, makes use of reciprocal form and force diagrams consisting of vertices, edges, and polyhedral cells. It offers an effective form-finding method for funicular structures whose members receive primarily axial forces under a proposed loading scenario.

Graphic statics can assist in the form-finding of funicular systems. While the form diagrams solved by graphic statics are primarily bar-node models with linear elements (Fig. 2a, b), research shows that they can be adapted as surface continuum models for ease of fabrication using sheet-based materials (Fig. 2c, d). Graphic statics also helps the design process of complex freeform concrete structures by offering an illustrated operation framework closely linked with fabrication methods while reflecting structural properties associated with the theory of plasticity (Schwartz, 2018). In addition, locations



**Fig. 2** Built projects designed with polyhedron-based 3D graphic statics: (a) a concrete spatial table (Akbarzadeh et al., 2021); (b) a concrete pavilion (Bolhassani et al., 2018); (c) a glass bridge (Lu, Seyedahmadian, et al., 2022); and (d) a paper bridge (Lu, Alsalem, & Akbarzadeh, 2022)

and magnitudes of the principal stress are annotated by the edges of the form diagram. Thus we will be able to reinforce the form accordingly.

Our proposal is in line with these endeavors to push forward the application of graphic statics by materializing certain walls of each polyhedral cell to create 3D-printable surfaces that would take and distribute the forces. By utilizing the notion of SFM, it aims to strengthen the connection between graphic-statics-driven design and materialization.

PolyFrame 2 (Lu, Hablicsek, & Akbarzadeh, 2024; Nejur & Akbarzadeh, 2021), a plug-in for Rhino (Robert McNeel & Associates, 2023b) and Grasshopper (Robert McNeel & Associates, 2023a), is a form-finding software based on the principles of graphic statics. The software takes a polyhedral force diagram as input and generates the reciprocal funicular form diagram using an iterative solver or an algebraic solver. Thus we are able to translate the funicular floor form-finding problem into designing an efficient polyhedral force diagram.

Zheng et al. (2020) utilizes machine learning to investigate the subdivision of a simple planar force diagram. In his work, the subdivided pattern is extruded to construct a 3D polyhedral force diagram, which then populates the efficient funicular form. Our work is based on one of his optimal outcomes which is claimed to reduce material usage by 51.7% (Fig. 3). Note that the funicular form is materialized into a ribbed floor where the funicular edges are *projected* to the top plane. The fabrication method of the system is not explored.

In this paper, we propose a compression-only unreinforced discrete system starting from the same subdivision force pattern. The design space covers one column, matching the force diagram explored in Zheng et al.

(2020). When repeating horizontally, the units form an aggregation as a compression-dominant funicular floor system. However, tension forces are needed at the boundaries of the floor system. The arrangement of the multi-span floor is beyond the scope of the paper. The one-column unit is fabricated as an SFM in our study. To further rationalize the materialization, the following adjustments are made to the force diagram (Fig. 4): The polyhedral cells are split in the middle to form two layers in the form diagram which become respectively the top and bottom edges of the polyhedral cells. The splitter is a sphere so that the polyhedral cells' vertical edges are gradually slanted towards the center (also seen in Fig. 10), similar to an unreinforced masonry vault system. Furthermore, the top half is replaced by extruding the new faces in the middle to the top surface so that the faces in between are perpendicular to the XY-plane. Thus the final form's top edges sit in the same XY-plane and make the cells flat to accommodate the flooring.

Additional post-processing to the form diagram is needed since the reciprocity determines the directions of the edges but not the length of them in certain configurations. The method to finalize this form is known as constraining the force or form diagram (Lu et al., 2024; Nejur & Akbarzadeh, 2018). We are specifically constraining the bottom 4 and outermost 8 vertices of the funicular form diagram to tailor the bounding dimensions of the system. With the help of the iterative constraint solver of PolyFrame 2, the symmetry of the system is also preserved. The result is a funicular mushroom floor where each column covers a  $2.6 \times 2.6$  m floor space.

Utilizing graphic statics, the form-finding process is direct and fast. It also gives us an opportunity to reinforce the area with maximal axial forces in the funicular form.

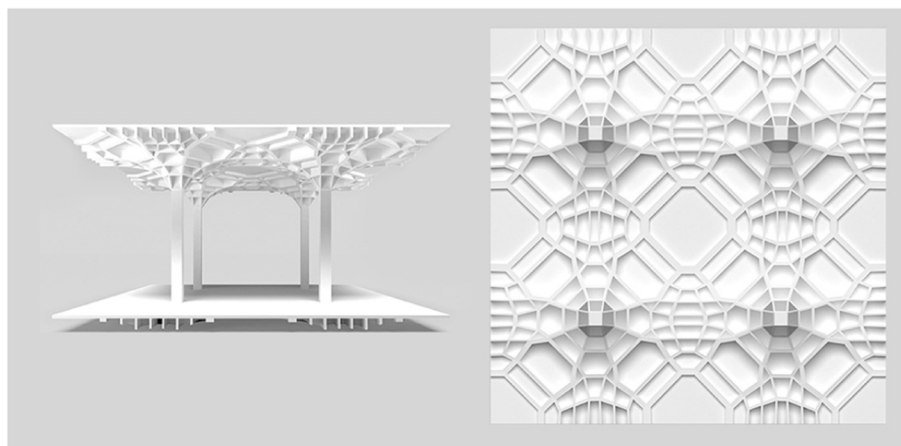


**Fig. 3** The funicular floor based on an optimal subdivision pattern generated through machine learning. Adapted from Zheng, Wang, Qi, Sun, and Akbarzadeh (2020)

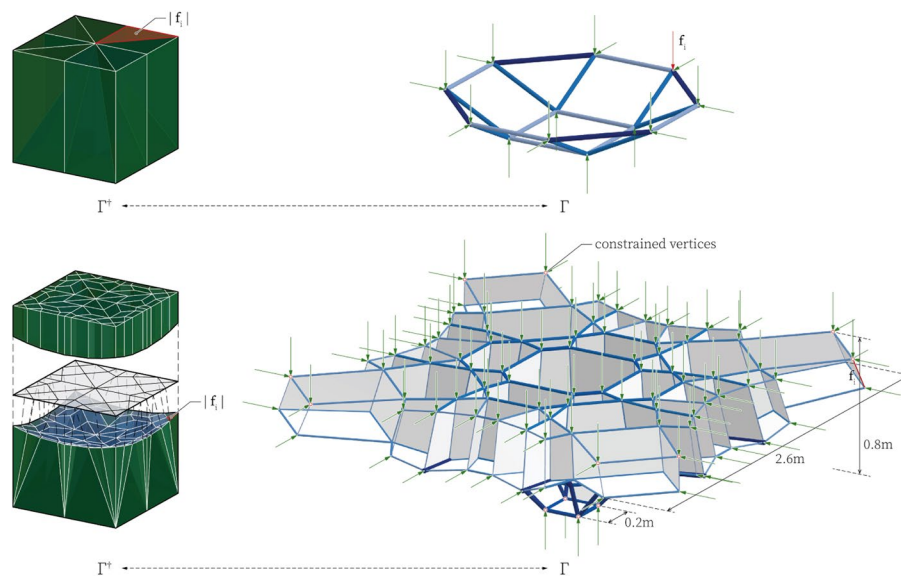


**Fig. 4** The graphic statics approach of form-finding: based on the force diagram ( $\Gamma^*$ ), a form diagram is found ( $\Gamma$ ). Top: a simple configuration; Bottom: a subdivided and adjusted configuration adopted in this paper

Later in Fig. 6 we can see the tailored reinforcement acts as an additional layer of rib in the system.

We revisit the ribbed floor system visualized by Fig. 3. Its simpler version can be seen in buildings where the entire span of the floor is cast in formworks over scaffoldings. The casting method restricts the floor's section geometry which can not have cavities. However, with 3D printing the creation of cavities is possible and materials can be assigned to the bottom of the funicular cells to better receive compressive forces and enhance the system's load-bearing capacity.

### 2.3 Force-informed toolpathing

An advantage of 3D printing is the selective deposition of material according to loading and stress conditions to increase material efficiency. For example, Tam and Mueller (2017) and Breseghello and Naboni (2022) assigned material along the stress lines to create efficient funicular forms. In our architectural 3D printing paradigm for producing shells, the deposition of material is also crucial. We propose a two-fold notion of force-informed toolpathing in deciding the printing schemes for compression-dominant components:

1. Solid printing: A solid geometry can be converted into layered toolpaths in different orientations. The anisotropic object (Fig. 5a) has a higher compressive strength in the printing direction (Z axis of the printed) compared to the other two directions (X, Y) (Ma et al., 2019; Xiao, Liu, & Ding, 2021a, 2021b). Therefore, when the geometry receives predominantly an

axial compressive force, its printing direction should align with the stress to maximize the strength of the structure (an example can be seen in Teng, Zhi, Yu, Yang, and Akbarzadeh (2023) where compressive and tensile forces are both discussed).

2. Contour printing: In architectural 3D printing, the creation of solid objects is often unnecessary and components are printed in layers as contours with optional infill patterns (Fig. 5b). The printing direction (Z) should also align with the stress for two reasons. Firstly the solid part has higher compressive strength in the Z direction. Secondly, in the X or Y direction, the geometry only has two continuum walls touching the two contact ends, and the rest material forms caps that do not pick up the compressive force.

The efficient toolpathing notion to harness the material printed can be summarized as “form follows force”. It directs the decisions in discretization and printing scheme development. The tailored slicing is not reflected in solid models produced by conventional desktop printers and can only be further examined in our proposed SFMs.

### 2.4 Discretization

The form generated using the graphic statics solver is accompanied by the direction and magnitude of the inner stresses. Following the notion of force-informed toolpathing the printing direction can be assigned aligning with the stress directions in our funicular model to

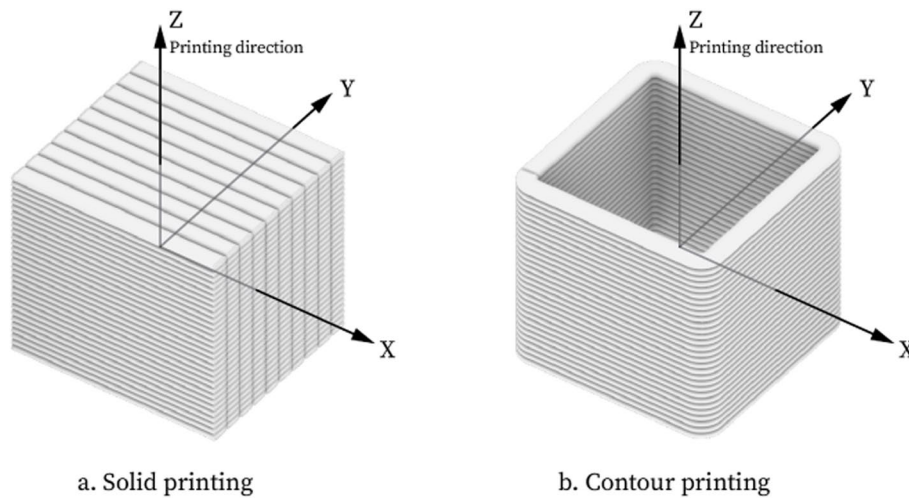


**Fig. 5** Different orientations in (a) solid printing and (b) contour printing

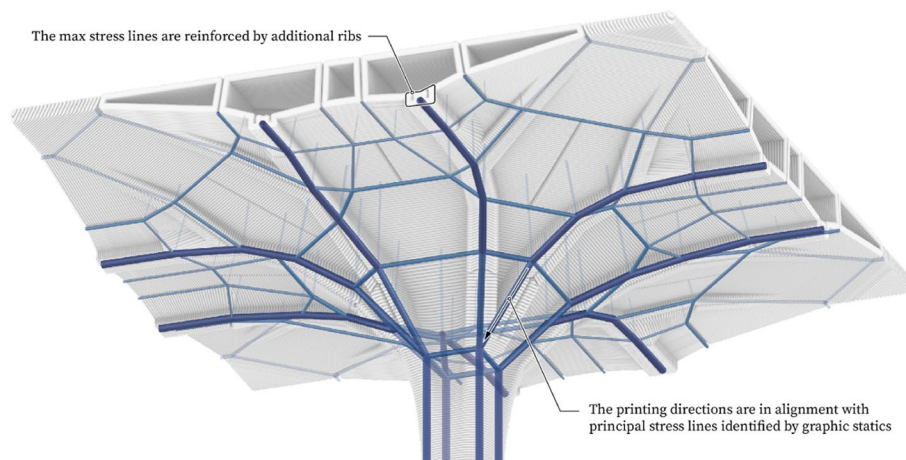
enhance their compressive strength. Figure 6 visualizes the cells and how their printing directions are aligned with the force. We also add additional corrugated ribs to the edges with max stresses for reinforcement. The alignment between printing and stress directions guides the discretization (Fig. 10) and slicing of all 62 pieces that formed the physical model of one column floor. It is further experimented in our rapid SFM production.

Another restriction of discrete systems is the size of elements to be manufactured and assembled. Therefore cells are inspected before orientation so that some small units with less axial forces are merged and some big units are split into two, resulting in acceptable and efficient sizes for construction-scale 3D printing.

### 2.5 Printing schemes

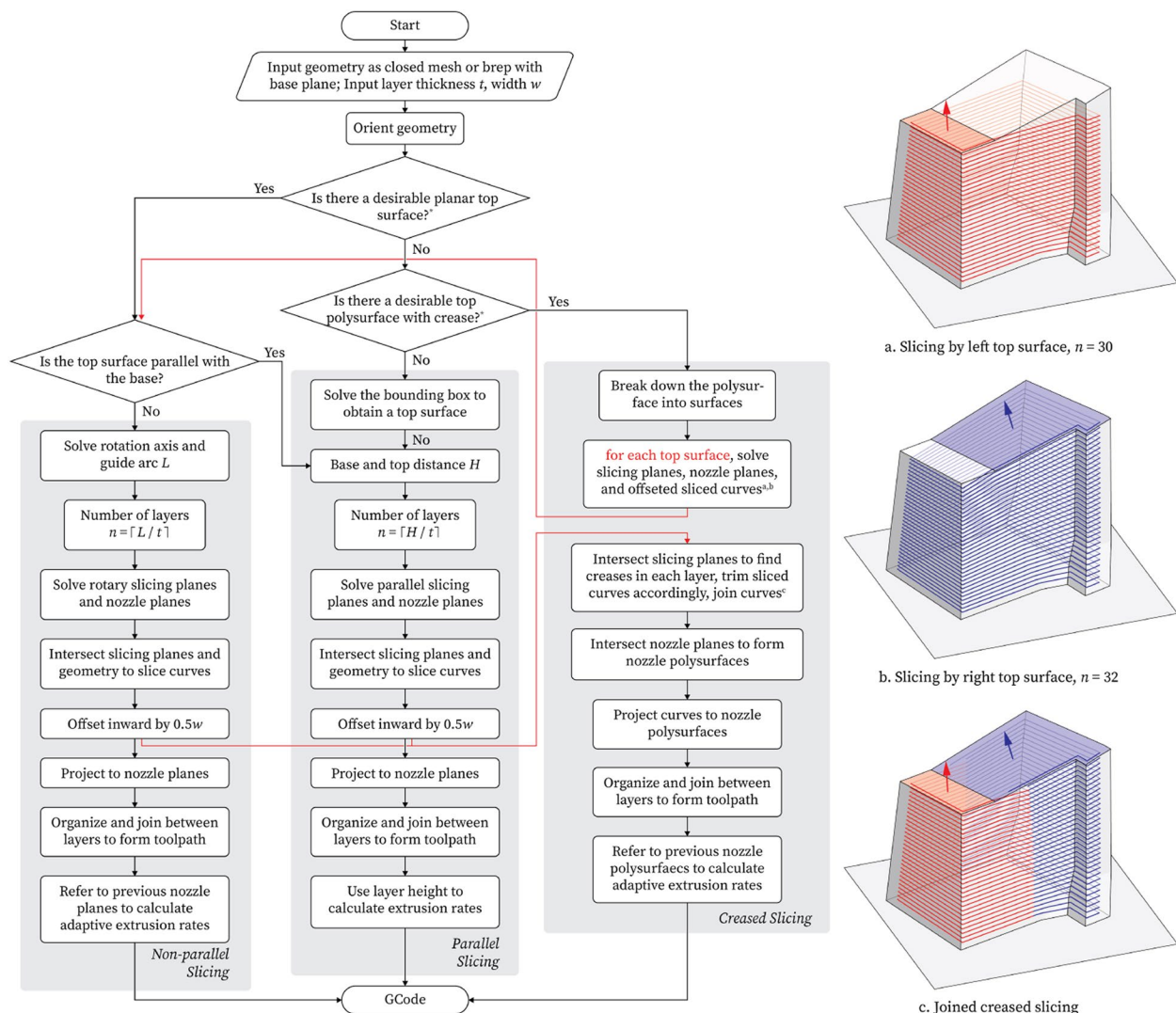
The design proposal employs a gantry printing system with a flat printbed. Therefore, the components are restricted to having flat bottom surfaces. On the other hand, not all surfaces/polysurfaces suit the criteria of being a cap that directs the slicing planes. The capping surface/polysurface should cover roughly the entire geometry to minimize areas acting as side caps that receive forces perpendicular to the printing direction (parallel with the layer plane). To prevent the creation of extremely thin layers that will corrupt the print quality, the angle between the top surfaces and base plane should not be too big, concerning the distance between them.

Figure 7 illustrates the details on determining the slicing method after a principal stress direction is given



**Fig. 6** Visualization of the assembled system showing the printed layers whose printing directions are aligned with principal stress lines suggested by the funicular form generated by graphic statics. The funicular form is visualized such that the section area is proportional to the axial force magnitude





\*A desirable top surface/polysurface covers roughly the entire geometry. The angle between each surface and the base plane should be within the non-planar printing restriction determined by the nozzle of the setup.

**Fig. 7** Left: The computational flowchart for determining slicing types (non-parallel, parallel or creased) and slicing to get the toolpath and GCode; Right: An example of creased slicing

and the geometry is oriented on the base plane chosen respectively. Three slicing methods are developed:

1. **Parallel Slicing:** Conventional slicing where each slicing plane is parallel to the bottom. Most commercial/consumer-level slicing software uses this default method. When dealing with vertically extruded structures it does not take full advantage of 3D printing systems and is thus known as 2.5D printing.
2. **Non-parallel Slicing:** The bottom and top faces are not parallel. They intersect at a rotating axis, around which a guide arc  $L$  starts from the centroid of the bottom face and ends at the top. The number of lay-

ers is calculated using  $L$  as the height in parallel slicing. The bottom plane is rotated around the axis to form the slicing planes in between.

3. **Creased Slicing:** A polysurface cap is identified. Referring to each face of the polysurface cap a set of curves are sliced using the non-parallel slicing method. The sets of curves are trimmed and joined to form the final curves. Note that for each surface the number of layers may vary. Due to that, the seam points where two sets of trimmed curves are connected are shifted from the location of the polysurface seam in the example shown by Figs. 7 and 8b.

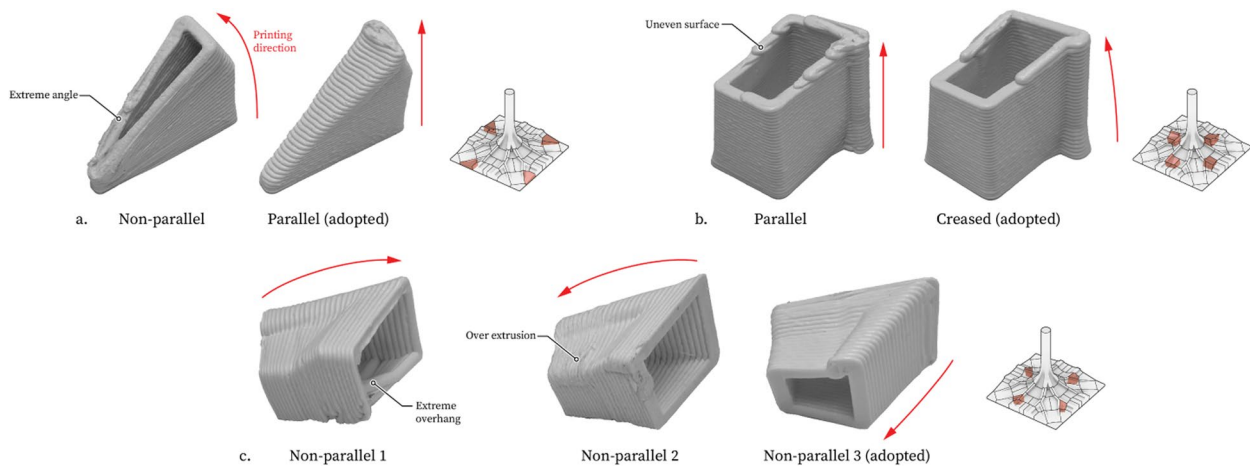


**Fig. 8** Comparative SFM component printing studies between (a) non-parallel and parallel slicing; (b) parallel and creased slicing; and (c) different non-parallel slicing configurations

The final post-process before printing is to connect the curves between layers and calculate the adaptive extrusion. A simple shell geometry usually has only one closed curve in each layer. They can be organized such that the cycling directions are the same (usually counter-clockwise) and their seam points are aligned to the previous. Based on those organized curves, a continuous curve that preserves the continuous finish of the print can be easily created. For the creased slicing where open curves take place at top layers, U-turn connections between layers are created and certain curves are flipped accordingly.

Adaptive extrusion refers to the local control of extrusion flow rate in the printing process. It has been utilized to achieve variable width for creating undulating surfaces (Yuan, Zhan, Wu, Beh, & Zhang, 2022; Zhan, Wu, Zhang, Yuan, & Gao, 2021) or avoiding overfills and underfills (Kuipers, Doubrovski, Wu, & Wang, 2020). In

the method of non-parallel slicing, adaptive extrusion helps realize the print's variable height. The height at a sample point is locally calculated as the distance from it to the previous slicing plane/polysurface. With the variable layer height information embedded in the toolpath, we can instruct an adaptive extrusion in the GCode to retain the same sectional width of 3 mm by changing the sectional area. Adaptive extrusion is key to matching the printed shell with the input geometry.

### 2.6 Design iterations with SFM

SFM can be produced once a primitive fabrication design is formed. To effectively visualize the design and test the fabrication details, we propose scaled printing tests in a sequence of three different scopes.

1. Component printing test: Fig. 8 illustrates how a cell can be assigned different orientations and slicing

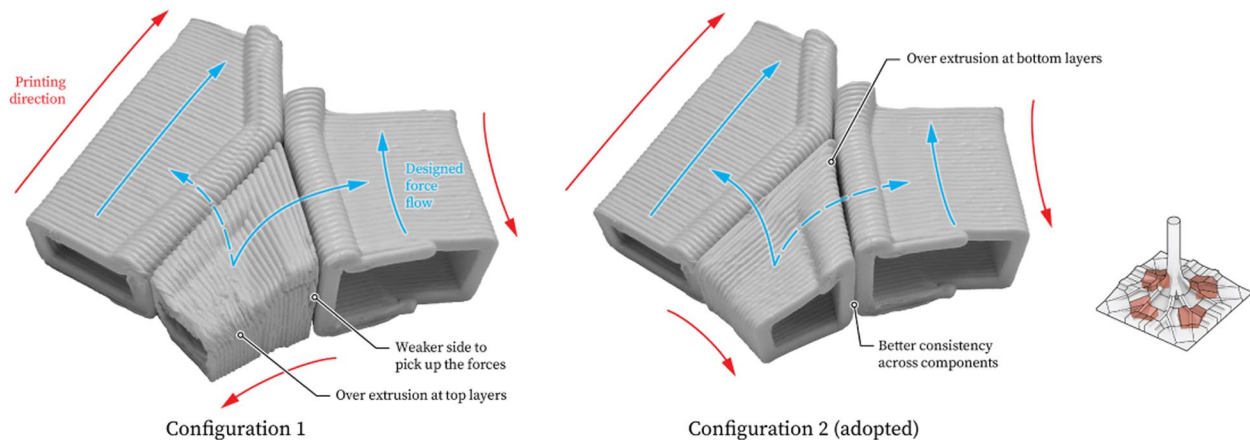


**Fig. 9** Partial SFM printing and assembly test with two different configurations

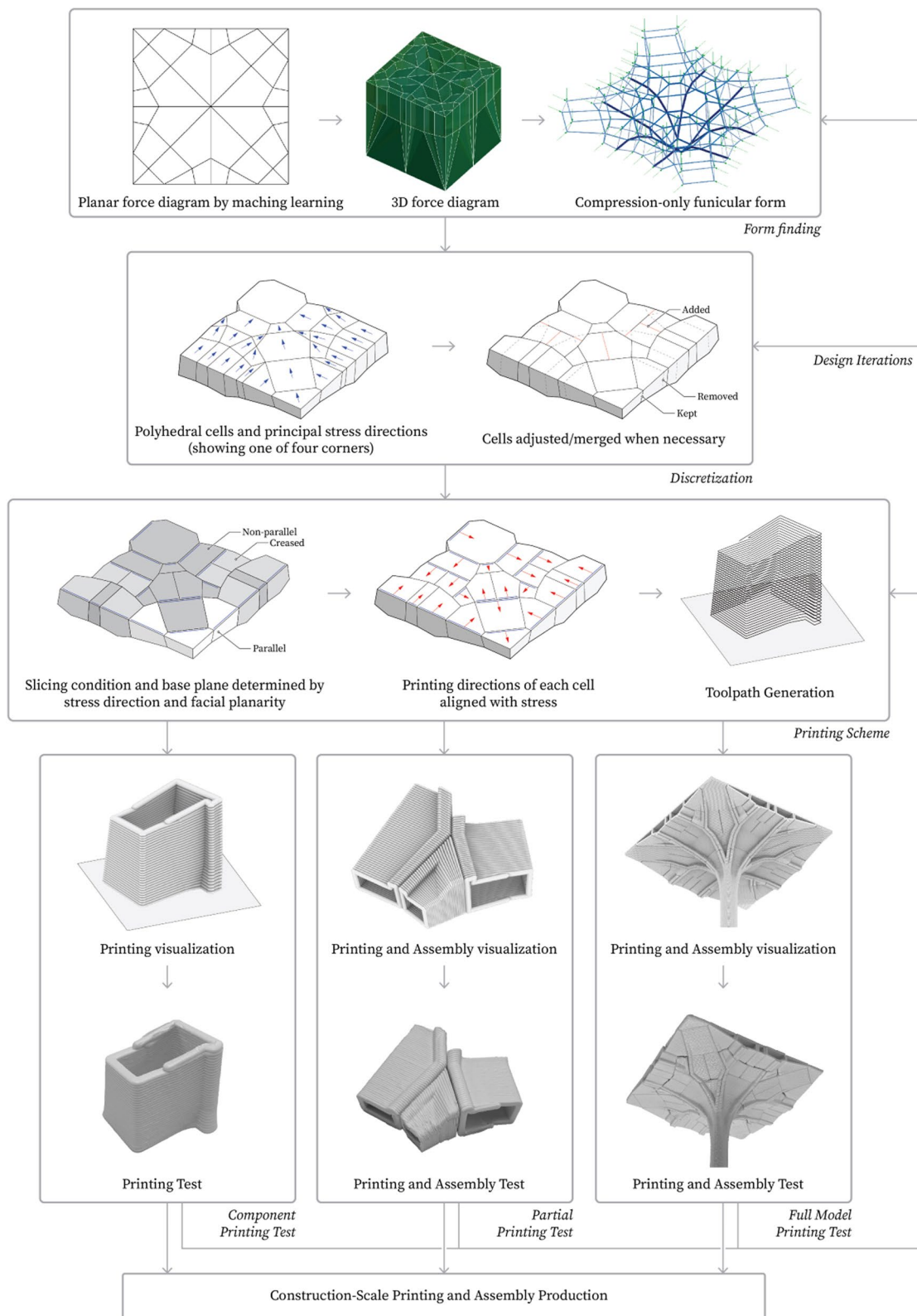


**Fig. 10** The proposed workflow from designing to prototyping the 3D-printed structural system

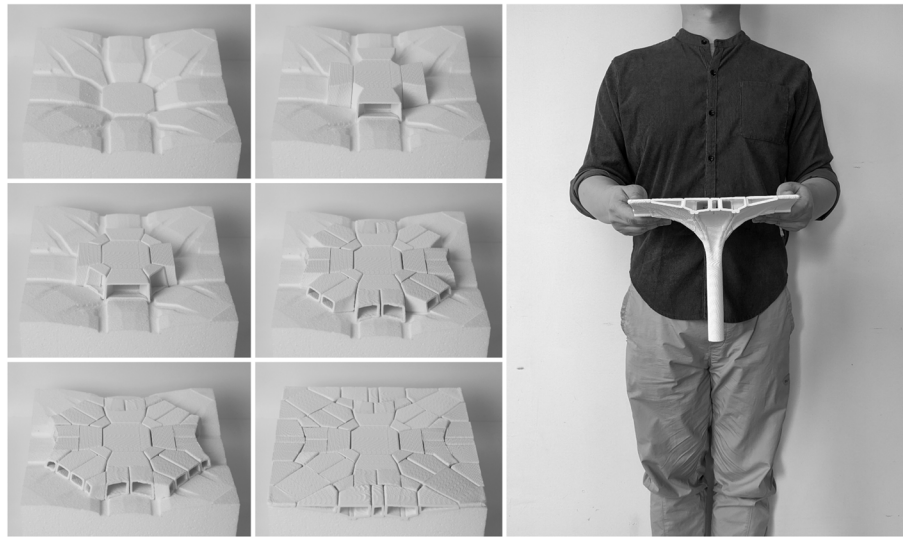


**Fig. 11** Left: The assembly sequence of the model; Right: The 26×26×25 cm model with its scale shown

**Table 2** Estimated cost for fabricating the components of our design in construction-scale robotic printing and in 1/10 desktop-scale SFM. Calibration and assembling costs are not included

	Construction scale production	1/10 desktop-scale SFM
Setup cost	\$150 000	\$200
Material Usage	2 000 kg Concrete	1 kg PET-G
Material cost	\$300	\$25
Printing Time	50 h	15 h
Energy consumption	750kWh	5kWh

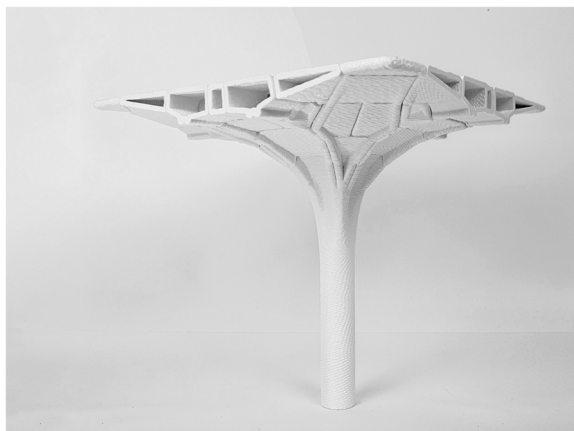


**Fig. 12** Physical prototype of the proposed funicular floor system with one column

methods. Figure 8a shows that a triangular piece with a 45° top surface has messy layer lines when printed non-parallelly due to the extreme angle. It can only be successfully printed with parallel slicing. Figure 8b shows how a component has poorly continuous top surfaces when it is printed using parallel slicing. However, when the slicing plane is rotated and creased to align with the top surfaces (also shown in Fig. 7), the finish quality is enhanced and the top matches the design more precisely. Figure 8c shows how different non-parallel slicing configuration raises the problem of extreme overhang and over extrusion. Such results are hard to precisely predict with modeling software and can be only captured by SFMs.

2. Partial printing test: Fig. 9 gives an example of printing part of the model to test contact surface quality. By checking the connectivity between adjacent components and consulting the force magnitude provided by graphic statics one can find an optimized solution for the discretization and printing scheme design and adjust the original form if necessary.
3. Full model printing test: After the design proposal has passed the previous two examinations, it is ready for a full model printing and assembly test. Building the SFM model also gives feedback to the construction-scale assembly proposal.

With the rapidly produced full model, it is also easier for communication between collaborators and clients.

Figure 10 gives an overview of our method from form-finding to materialization and fabrication of the

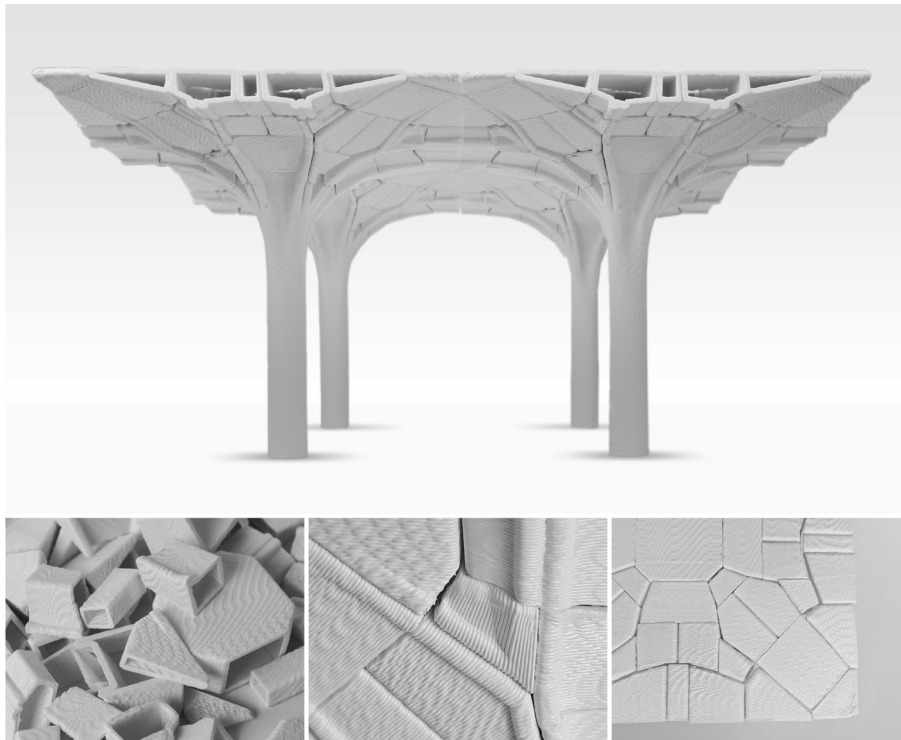


**Fig. 13** Top: The proposed system organized by four columns; Bottom: discrete blocks, detail, and top view of the floor

system. By incorporating graphic statics with 3D printing rationales, it fully demonstrates the potential of SFM in prototyping innovative 3D-printed concrete structural systems.

### 3 Results

The full model consists of 62 3D-printed components. The pieces are then assembled according to a CNC-milled foam base simulating the scaffolding using glue. The assembly sequence of the compression-only system starts from the center, as in a masonry vault structure (Fig. 11).

As presented in Table 2, it is proven that designing 3D-printed concrete structures using SFM is a cost-effective approach. The setup cost of a desktop 3D printer is low. Less material is required to print small-scale models, minimizing material usage and cost. Smaller models also have shorter printing times so that more design iterations can be evaluated. Desktop 3D printers also typically consume little energy relative to industrial systems, not to mention the labor saved in processing the material and maintaining the workspace. Given the low overhead in terms of both economic and material resources needed for desktop-scale SFM versus full-scale fabrication, the proposed method enables an agile design-fabrication process.

The built model (Figs. 12, 13) demonstrates the idea of aligning the form with force and makes possible a close investigation into the strength and limits of such structures. The ribbed part realized by the U-shaped profile of the toolpath adds to both structural strength and the aesthetic of the system as they highlight the idea of “form follows force”.

### 4 Conclusion and future work

#### 4.1 Contribution of the study

The contribution of the study is three-fold. It introduces the concept of SFM as opposed to conventional smooth models and proposes the usage of SFM to bridge the gap between geometrical and fabrication design and streamline the design iterations in 3D-printed discrete concrete structures. It provides an accessible and affordable platform for printing SFMs and presents slicing methods compatible with different geometries.

The case study of the funicular floor showcases the rapid design iterations made possible by producing SFMs on three different scopes: component, partial model, and full model. It sets a paradigm for efficiently rationalizing discrete 3D-printed concrete structures. The method can be adapted to different design tasks and facilitate communication between architects, engineers, and clients.

By adopting the form-finding approach of polyhedron-based graphic statics and aligning the printing direction with the stress, this case study celebrates the notion of force-informed toolpathing and illustrates SFM's ability to help realize design research in architectural 3D printing.

#### 4.2 Limitations

Currently the application of SFM is limited by the following aspects. The commercially available desktop printers tested in this study have 3 translational degrees of freedom (DOF) while robotic printing systems have 6 DOFs. The SFM method with such printers does not reflect the effect of rotating nozzles, inclined nozzles, and non-standard nozzles seen in robotic printing systems.

Printing schemes can be tested effectively in SFMs to show if they are collision-free, recreate the desired surfaces, and demonstrate consistent layer lines. However, materials used in SFMs and construction-scale concrete printing are different, resulting in different limits in printable overhangs of the toolpaths. In that regard, being able to be printed as SFM, especially using thermoplastic filaments, does not guarantee a successful print on a construction scale. Furthermore, concrete printing typically experiences a 2% linear shrinkage during the curing process (Zhang & Xiao, 2021) and is thus suspect to cracking. This issue is not reflected in SFMs. In using SFMs as verification, the designers and engineers need to resort to past experience to prevent such possible defects before moving on to the full scale.

For exploratory design iterations, SFMs are informative companions to designers. However, to facilitate construction tasks, quantitative metrics for evaluating SFM tests need to be established.

#### 4.3 Future work

To further harness the advantages of SFM, this study can be expanded in the following aspects. The slicing and printing methods and the physical setup can be upgraded such that advanced 3D printing methods including non-planar printing (Anton, Skevaki, Bischof, Reiter, & Dillenburger, 2022; Mitropoulou, Bernhard, & Dillenburger, 2020, 2022), multi-axis printing (Dai et al., 2018; Fang et al., 2020; Li et al., 2022), and continuous printing (Zhao et al., 2016) can also be tested in SFMs. Implementing those methods in SFM verifies their viability in producing 3D-printed concrete structural components.

The method of SFM can be applied to discrete concrete systems with complex fabrication details such as bolts and nuts and post-tensional cables. The interface between the standard metal hardware and the toolpath (for example, conduits for post-tensioning cables in Fig. 1a, c, d) can be investigated using SFM.

Cross-scale quantitative criteria for assessing the printability and finish quality of the components can be developed. To do so, a series of controlled printing experiments can be conducted where the SFMs then undergo numerical examinations using methods such as digital image correlation.

Alternative materials can be investigated in producing SFMs. Different types of thermoplastics, customized concrete recipes, and other materials can be tested and their advantages, limitations, and resemblance to regular concrete can be comparatively studied. By printing with a material that has the closest density and rheology to concrete, one can effectively test the material behavior of the deposition using SFM and thus further verify the printability of the construction scale components.

#### Acknowledgements

This research was supported by the Future Eco Manufacturing Research Grants (NSF FMRG-2037097 CMMI) and Faculty Early Career Development Program (NSF CAREER-1944691 CMMI) of the U.S. National Science Foundation and the Advanced Research Projects Agency–Energy (ARPA-E) Grant of the U.S. Department of Energy (DE-AR0001631) awarded to Dr. Masoud Akbarzadeh. The authors would like to thank Yi (Simone) Yang for the assistance in model making and Dr. Maximilian E. Ororbia for the writing suggestions.

#### Authors' contributions

Yefan Zhi: Conceptualization, Methodology, Software, Formal analysis, Investigation, Writing—Original Draft, Writing—Review & Editing, Visualization, Project administration. Teng Teng: Conceptualization, Methodology, Writing—Review & Editing. Masoud Akbarzadeh: Conceptualization, Resources, Supervision, Funding acquisition, Writing—Review & Editing.

#### Declarations

##### Competing interests

There is no competing interest in this publication and research.

Received: 11 March 2024 Accepted: 8 July 2024

Published: 8 August 2024

#### References

- Ahmed, Z., Wolfs, R., Bos, F., Salet, T. (2022). A framework for large-scale structural applications of 3D printed concrete: the case of a 29 m bridge in the netherlands. *Open Conference Proceedings*, 1, 5–19. <https://doi.org/10.52825/ocpv1i.74>
- Akbarzadeh, M. (2016). *3D Graphical Statics Using Reciprocal Polyhedral Diagrams*. Zurich: ETH Zurich. <https://doi.org/10.3929/ethz-a-010867338>
- Akbarzadeh, M., Tabatabaie Ghomi, A., Bolhassani, M., Akbari, M., Seyedahmadian, A., Sun, J., Yao, H., Miziumski, J., & Papalexou, K. (2021). Saltatur: Node-based assembly of funicular spatial concrete. In M. Yablonina, A. Marcus, S. Doyle, M. del Campo, V. Ago & B. Slocum (Eds.), *Proceedings of the 40th Annual Conference of the Association for Computer-Aided Design in Architecture (ACADIA)* (pp. 108–113). Virtual Conference: Association for Computer-Aided Design in Architecture (ACADIA)
- Anton, A., Skevaki, E., Bischof, P., Reiter, L., Dillenburger, B. (2022). Column-Slab Interfaces for 3D Concrete Printing. In Masoud Akbarzadeh and Dorit Aviv and Hina Jamelle and Robert Stuart-Smith (Eds.), *Proceedings of the 42nd Annual Conference of the Association for Computer-Aided Design in Architecture (ACADIA)* (Vol. 1, pp. 58–67). Philadelphia, PA: Association for Computer-Aided Design in Architecture (ACADIA)
- Bhooshan, S. (2022). *Shape Design of 3D-Concrete-Printed Masonry Structures*. Zurich: ETH Zurich. <https://doi.org/10.3929/ethz-b-000614010>

- Bolhassani, M., Akbarzadeh, M., Mahnia, M., & Taherian, R. (2018). On structural behavior of a funicular concrete polyhedral frame designed by 3D graphic statics. *Structures*, *14*, 56–68. <https://doi.org/10.1016/j.jstruc.2018.02.002>
- Bos, F., Wolfs, R., Ahmed, Z., & Salet, T. (2016). Additive manufacturing of concrete in construction: Potentials and challenges of 3D concrete printing. *Virtual and Physical Prototyping*, *11*(3), 209–225. <https://doi.org/10.1080/17452759.2016.1209867>
- Breseghele, L., & Naboni, R. (2022). Toolpath-based design for 3D concrete printing of carbon-efficient architectural structures. *Additive Manufacturing*, *56*, 102872. <https://doi.org/10.1016/j.addma.2022.102872>
- Dai, C., Wang, C. C. L., Wu, C., Lefebvre, S., Fang, G., & Liu, Y.-J. (2018). Support-free volume printing by multi-axis motion. *ACM Trans. Graph.*, *37*(4), 134. <https://doi.org/10.1145/3197517.3201342>
- De Luca, L., Veron, P., & Florenzano, M. (2006). Reverse engineering of architectural buildings based on a hybrid modeling approach. *Computers & Graphics*, *30*(2), 160–176. <https://doi.org/10.1016/j.cag.2006.01.020>
- Fang, G., Zhang, T., Zhong, S., Chen, X., Zhong, Z., & Wang, C. C. L. (2020). Reinforced FDM: Multi-axis filament alignment with controlled anisotropic strength. *ACM Trans. Graph.*, *39*(6), 204. <https://doi.org/10.1145/3414685.3417834>
- Gosselin, C., Duballet, R., Roux, P., & Gaudillière-Jami, N., Dirrenberger, J., Morel, P. (2016). Large-scale 3D printing of ultra-high performance concrete – a new processing route for architects and builders. *Materials & Design*, *100*, 102–109. <https://doi.org/10.1016/j.matdes.2016.03.097>
- Jain, P., & Kuthe, A. (2013). Feasibility study of manufacturing using rapid prototyping: FDM approach. *Procedia Engineering*, *63*, 4–11. <https://doi.org/10.1016/j.proeng.2013.08.275>
- Khoshevis, B. (2004). Automated construction by contour crafting—related robotics and information technologies. *Automation in Construction*, *13*(1), 5–19. <https://doi.org/10.1016/j.autcon.2003.08.012>
- Kuipers, T., Doubrovski, E.L., Wu, J., Wang, C.C. (2020). A framework for adaptive width control of dense contour-parallel toolpaths in fused deposition modeling. *Computer-Aided Design*, *128*, 102907. <https://doi.org/10.1016/j.cad.2020.102907> Retrieved from <https://www.sciencedirect.com/science/article/pii/S0010448520301007>
- Li, Y., He, D., Yuan, S., Tang, K., & Zhu, J. (2022). Vector field-based curved layer slicing and path planning for multi-axis printing. *Robotics and Computer-Integrated Manufacturing*, *77*, 102362. <https://doi.org/10.1016/j.rcim.2022.102362>
- Li, Y., Wu, H., Xie, X., Zhang, L., Yuan, P. F., & Xie, Y. M. (2024). FloatArch: A cable-supported, unreinforced, and re-assemblable 3D-printed concrete structure designed using multi-material topology optimization. *Additive Manufacturing*, *81*, 104012. <https://doi.org/10.1016/j.addma.2024.104012>
- Lu, Y., Alsalem, T., Akbarzadeh, M. (2022). A Method for Designing Multi-Layer Sheet-Based Lightweight Funicular Structures. *Journal of the International Association for Shell and Spatial Structures*, *63* (4), 252–262. <https://doi.org/10.20898/j.iaass.2022.018>
- Lu, Y., Hablicsek, M., Akbarzadeh, M. (2024). Algebraic 3D graphic statics with edge and vertex constraints: A comprehensive approach to extend the solution space for polyhedral form-finding. *Computer-Aided Design*, *166*, 103620. <https://doi.org/10.1016/j.cad.2023.103620>
- Lu, Y., Seyedahmadian, A., Chhadeh, P.A., Cregan, M., Bolhassani, M., Schneider, J., ... Akbarzadeh, M. (2022). Funicular glass bridge prototype: design optimization, fabrication, and assembly challenges. *Glass Structures & Engineering*, *7* (2), 319–330. <https://doi.org/10.1007/s40940-022-00177-x>
- Ma, G., Li, Z., Wang, L., Wang, F., & Sanjayana, J. (2019). Mechanical anisotropy of aligned fiber reinforced composite for extrusion-based 3D printing. *Construction and Building Materials*, *202*, 770–783. <https://doi.org/10.1016/j.conbuildmat.2019.01.008>
- Mitropoulou, I., Bernhard, M., Dillenburger, B. (2020). Print paths key-framing: Design for non-planar layered robotic FDM printing. In Emily Whiting, John Hart, Cynthia Sung, Nadya Peek, Masoud Akbarzadeh, Dan Aukes, Adriana Schulz, Hayden Taylor & Jeeun Kim (Eds.), *Proceedings of the 5th Annual ACM Symposium on Computational Fabrication* (pp. 1–10). New York, NY: Association for Computing Machinery. <https://doi.org/10.1145/3424630.3425408>
- Mitropoulou, I., Bernhard, M., Dillenburger, B. (2022). Nonplanar 3D printing of bifurcating forms. *3D Printing and Additive Manufacturing*, *9* (3), 189–202. <https://doi.org/10.1089/3dp.2021.0023>
- Nejur, A., & Akbarzadeh, M. (2018). Constrained manipulation of polyhedral systems. In Caitlin Mueller & Sigrid Adriaenssens (Eds.), *Proceedings of IASS Annual Symposia* (pp. 1–8). Boston, MA: International Association for Shell and Spatial Structures (IASS)
- Nejur, A., & Akbarzadeh, M. (2021). Polyframe, efficient computation for 3D graphic statics. *Computer-Aided Design*, *134*, 103003. <https://doi.org/10.1016/j.cad.2021.103003>
- Niknafs Kermani, N., Advani, S. G., & F'erec, J. (2023). Orientation predictions of fibers within 3D printed strand in material extrusion of polymer composites. *Additive Manufacturing*, *77*, 103781. <https://doi.org/10.1016/j.addma.2023.103781>
- Ooms, T., Vantighem, G., Tao, Y., Bekaert, M., De Schutter, G., Van Tittelboom, K., De Corte, W. (2022). The production of a topology-optimized 3d-printed concrete bridge. *Third RILEM International Conference on Concrete and Digital Fabrication*.
- Paolini, A., Kollmannsberger, S., & Rank, E. (2019). Additive manufacturing in construction: A review on processes, applications, and digital planning methods. *Additive Manufacturing*, *30*, 100894. <https://doi.org/10.1016/j.addma.2019.100894>
- Robert McNeel & Associates (2023a). *Grasshopper*. <https://www.rhino3d.com/learn/?query=kind%20grasshopper&modal=null>
- Robert McNeel & Associates (2023b). *Rhinoceros 3D*. <https://www.rhino3d.com/>
- Schwartz, J. (2018). Graphic statics and their potential for digital design and fabrication with concrete. *Cement and Concrete Research*, *112*, 122–135. <https://doi.org/10.1016/j.cemconres.2018.06.015>
- Sharif, S., & Gentry, T.R. (2015). Design cognition shift from craftsman to digital maker. In Y. Ikeda, C. M. Herr, D. Holzer, S. Kajima, M. J. Kim & M. A. Schnabel (Eds.), *Proceedings of the 20th International Conference of the Association for Computer-Aided Architectural Design Research in Asia (CAADRIA 2015)* (pp. 683–692). Hong Kong: Association for Computer-Aided Architectural Design Research in Asia (CAADRIA). <https://doi.org/10.52842/conf.caadria.2015.683>
- Tam, K.-M.M., & Mueller, C. (2017). Additive manufacturing along principal stress lines. *3D Printing and Additive Manufacturing*, *4*, 63–81. <https://doi.org/10.1089/3dp.2017.0001>
- Teng, T., Zhi, Y., Yu, K.-H., Yang, S., Akbarzadeh, M. (2023). Continuous multi-filament 3D printing for tension-compression structure components. In Y.M. Xie, J. Burry, T.U. Lee & J. Ma (Eds.), *Proceedings of IASS 2023 symposium Integration of Design and Fabrication* (pp. 126–138). Melbourne: International Association for Shell and Spatial Structures (IASS)
- Vantighem, G., De Corte, W., Shakour, E., & Amir, O. (2020). 3D printing of a post-tensioned concrete girder designed by topology optimization. *Automation in Construction*, *112*, 103084. <https://doi.org/10.1016/j.autcon.2020.103084>
- van Woensel, R., van Oirschot, T., Burgmans, M., Mohammadi, M., Hermans, K. (2018). Printing architecture: An overview of existing and promising additive manufacturing methods and their application in the building industry. *The International Journal of the Constructed Environment*, *9*, 57–81. <https://doi.org/10.18848/2154-8587/CGP/v09i01/57-81>
- Viswanathan, V., & Linsey, J. (2011). Understanding physical models in design cognition: A triangulation of qualitative and laboratory studies. *2011 Frontiers in Education Conference (FIE)* (pp. S3F-1–S3F-6). Rapid City, SD: IEEE. <https://doi.org/10.1109/FIE.2011.6142848>
- Wu, H., Li, Z., Zhou, X., Wu, X., Bao, D.W., Yuan, P. (2022). Digital design and fabrication of a 3d concrete printed funicular spatial structure. In Jeroen van Ameijde, Nicole Gardner, Kyung Hoon Hyun, Dan Luo & Urvi Sheth (Eds.), *Proceedings of the 27th International Conference on Computer-Aided Architectural Design Research in Asia (CAADRIA 2022)* (Vol. 2, pp. 71–80). Sydney: Association for Computer-Aided Architectural Design Research in Asia (CAADRIA). <https://doi.org/10.52842/conf.caadria.2022.2.071>
- Xiao, J., Ji, G., Zhang, Y., Ma, G., Mechtcherine, V., Pan, J., Du, S. (2021). Large-scale 3D printing concrete technology: Current status and future opportunities. *Cement and Concrete Composites*, *122*, 104115. <https://doi.org/10.1016/j.cemconcomp.2021.104115>
- Xiao, J., Liu, H., & Ding, T. (2021b). Finite element analysis on the anisotropic behavior of 3D printed concrete under compression and flexure. *Additive Manufacturing*, *39*, 101712. <https://doi.org/10.1016/j.addma.2020.101712>
- Yuan, P.F., Zhan, Q., Wu, H., Beh, H.S., Zhang, L. (2022). Real-time toolpath planning and extrusion control (rtpec) method for variable-width 3d concrete printing. *Journal of Building Engineering*, *46*, 103716. <https://doi.org/10.1016/j.jbe.2022.103716>

- [org/10.1016/j.jobe.2021.103716](https://doi.org/10.1016/j.jobe.2021.103716) Retrieved from <https://www.sciencedirect.com/science/article/pii/S2352710221015746>
- Zhan, Q., Wu, H., Zhang, L., Yuan, P., Gao, T. (2021). 3d concrete printing with variable width filament. *The 39th Conference on Education and Research in Computer Aided Architectural Design in Europe (eCAADe)* (Vol. 2, p. 153–160). Novi Sad: Education and research in Computer Aided Architectural Design in Europe (eCAADe). <https://doi.org/10.52842/conf.ecaade.2021.2.153>
- Zhang, H., & Xiao, J. (2021). Plastic shrinkage and cracking of 3d printed mortar with recycled sand. *Construction and Building Materials*, 302, 124405, <https://doi.org/10.1016/j.conbuildmat.2021.124405> Retrieved from <https://www.sciencedirect.com/science/article/pii/S0950061821021632>
- Zhao, H., Gu, F., Huang, Q.-X., Garcia, J., Chen, Y., Tu, C., .Chen, B. (2016). Connected fermat spirals for layered fabrication. *ACM Trans. Graph.*, 35 (4), <https://doi.org/10.1145/2897824.2925958>
- Zheng, H., Wang, X., Qi, Z., Sun, S., Akbarzadeh, M. (2020). Generating and optimizing a funicular arch floor structure. In B. Slocum, V. Ago, S. Doyle, A. Marcus, M. Yablonina & M. del Campo (Eds.), *Proceedings of the 40th Annual Conference of the Association for Computer-Aided Design in Architecture (ACADIA)* (Vol. 1, pp. 208–217). Virtual Conference: Association for Computer-Aided Design in Architecture (ACADIA). <https://doi.org/10.52842/conf.acadia.2020.2.208>

### Publisher's Note

Springer Nature remains neutral with regard to jurisdictional claims in published maps and institutional affiliations.